

Stability of the wall jet formed by the impingement of a single-phase jet

İ. B. ÖZDEMİR (İSTANBUL)

THIS PAPER DESCRIBES a theoretical investigation of the possibility that the large structures of the wall jet flow formed after oblique impingement of an axisymmetric jet were generated by the flow instabilities, so that the experimentally reported discrete frequencies were synonymous with instability modes. The wall jet flow was triple-decomposed into a time-independent, pseudolaminar motion defined by the time-averaged velocity field, upon which incoherent and coherent turbulent fluctuations were superimposed. Solution of the inviscid, one-dimensional flow equations with large coherent structures, which were modelled by spatially evolving waves, was given in detail and revealed that the distribution of the radial fluctuation intensity and the frequency of large structures compare well with the experiments justifying the deterministic nature of the coherent motion.

Notations

Symbols

A_p, A_r, A_z, A_ϕ	amplitude modulation functions,
f	real-valued frequency,
$\mathcal{F}(f)$	complex amplitude of the rotating vector defined in Eq. (4.2),
H	nozzle-to-plate distance,
i	$\sqrt{-1}$,
m	real-valued azimuthal wavenumber,
p	parameter defined in Eq. (3.2),
\tilde{p}	coherent pressure fluctuation,
p'	incoherent pressure fluctuation,
P	instantaneous value of pressure,
\bar{P}	time-averaged value of pressure,
$\mathbb{P}(f)$	total power associated with frequency f ,
r	radial coordinate defined from geometrical impingement point,
r_w	wetted radius defined in Eq. (2.3),
Re	Reynolds number,
s	parameter defined in Eq. (3.1),
t	time,
$\tilde{u}_r, \tilde{u}_z, \tilde{u}_\phi$	components of coherent velocity fluctuations in three directions,
u'_r, u'_z, u'_ϕ	components of incoherent velocity fluctuations in three directions,
U_r, U_z, U_ϕ	components of instantaneous velocity field in three directions,
$\bar{U}_r, \bar{U}_z, \bar{U}_\phi$	components of time-averaged velocity field in three directions,
$\bar{U}_{r,M}$	maximum of the time-averaged radial velocity component,
z	coordinate normal to the plate,
$z_{0.5}$	wall distance at which time-averaged radial velocity attains half of the maximum value,
$()^*$	superscript refers to nondimensional form of variables.

Greek Symbols

α	complex-valued wavenumber,
α_i	imaginary part of α ,
α_r	real part of α ,
β	real-valued circular frequency ($2\pi f$),
η	parameter defined in Eq. (3.1),
γ	half-cone angle of the inflowing jet,
λ	wavelength of the educed coherent structures,
ν	kinematic viscosity of the air,
ϕ	azimuthal coordinate,
ρ	density of the air,
σ	parameter defined in Eq. (3.2),
θ	angle of impingement,
ζ	parameter defined in Eq. (3.2),
τ	parameter defined in Eq. (3.2).

1. Introduction

THE RADIAL WALL JET formed after impingement of an axisymmetric jet on a flat surface has been of interest in many engineering applications, including heat or mass transfer to or from the flow, and the interaction between the pressure waves radiating from the plate and coherent structures of the inflowing jet. In response to these enquiries, time-averaged flow fields have been explored for normal impingement usually in the vicinity of the stagnation region, but knowledge of the downstream evolution of the flow has remained elusive. Recently, the radial wall jet has attracted particular attention in terms of instantaneous patterns of large structures (HO and NOSSEIR [1, 2], LANDRETH and ADRIAN [3]) whose characteristic dimensions are commensurate with the width of the wall jet and lead to the time-averaged flow field with higher turbulence intensities (POREH, TSUEI and CERMAK [4]) than in aerodynamic boundary layers. ÖZDEMİR and WHITELAW [5] investigated the downstream evolution of the time-averaged and instantaneous flow fields of a radial wall jet formed after oblique impingement of an axisymmetric jet, and showed that the symmetry of the toroidal vortices (DIDDEN and HO [6]) was distorted as impingement deviated from normal, resulting in a complex cluster of concentric yet asymmetric toroidal vortices.

It is known (HO and HUERRE [7]) that the evolution of vortical structures in laminar and turbulent shear layers is governed by essentially the same dynamical processes, so that the concepts of hydrodynamic stability can be applied to turbulent shear layers. Inflectional instability of the shear layers has taken a great deal of attention, as for example GREGORY, STUART and WALKER [8] and STUART [9], because disturbances generated near the point of inflection could dominate the fluctuations and propagate at a speed smaller than the corresponding velocity at the inflection point. HOWARD [10] and TSUJI *et al.* [11] argued that the number of

distinct unstable disturbances associated with the inflection points could not exceed the number of neutral modes. The roll-up of travelling instability waves into the periodic array of vortices in a plane mixing layer was studied by MICHALKE [12] and MICHALKE and HERMANN [13] in that the evolution of disturbances in the basic flow direction seemed to be better modelled by spatially growing disturbances and, when the width of the flow region varied considerably, quantities controlled by the history of the flow development required an additional scaling parameter to account for the coordinate stretching (BOUTHIER [14], GASTER [15], CRIGHTON and GASTER [16]).

The purpose of the present study was to examine the possibility that the large vortical structures observed by ÖZDEMİR and WHITELAW [5] in their radial wall jet were generated by the flow instabilities, so that the discrete frequencies measured were synonymous with instability modes. The conjecture that the wall jet flow was not so obviously nonlinear gave impetus to the present linear analysis and should not be far from reality, since the array of vortices observed was discrete and no nonlinear vortex interaction processes, such as vortex pairing or tearing as described by HUSSAIN [17], were observed.

2. Equations for coherent structures

It can be envisaged that large scale motion of the wall jet was caused by deterministic instability waves which were, together with stochastic background fluctuations, superimposed on the pseudolaminar flow defined by the time-averaged velocity field. Therefore, since the wall flow was temporarily stationary, an instantaneous quantity can be decomposed into a time-independent mean, a coherent and an incoherent turbulence quantities (HUSSAIN [17], HUSSAIN and REYNOLDS [18]) and, in cylindrical coordinates, the instantaneous velocity vector can be given as (see Fig. 1, for the coordinate system and the flow domain)

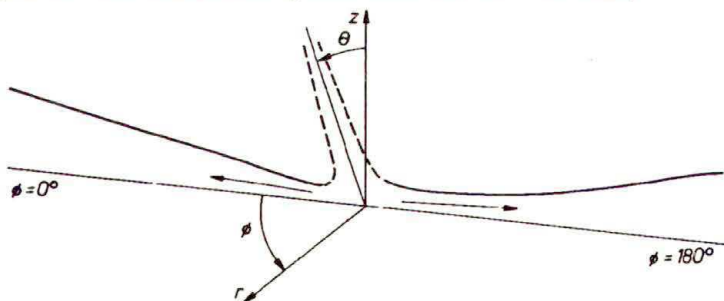


FIG. 1. Schematic of the flow configuration.

$$\begin{aligned}
 U_r(r, \phi, z, t) &= \bar{U}_r(r, \phi, z) + \tilde{u}_r(r, \phi, z, t) + u'_r(r, \phi, z, t), \\
 U_\phi(r, \phi, z, t) &= \tilde{u}_\phi(r, \phi, z, t) + u'_\phi(r, \phi, z, t), \\
 U_z(r, \phi, z, t) &= \bar{U}_z(r, \phi, z) + \tilde{u}_z(r, \phi, z, t) + u'_z(r, \phi, z, t),
 \end{aligned}
 \tag{2.1}$$

with the pressure field

$$P(r, \phi, z, t) = \overline{P}(r, \phi, z) + \tilde{p}(r, \phi, z, t) + p'(r, \phi, z, t),$$

where the over-bar, tilda and prime refer the quantities for the mean flow, the coherent (wave motion) and incoherent (random) turbulent fluctuations, respectively. Note that, based on the surface flow visualisation experiments [5], the mean azimuthal velocity, \overline{U}_ϕ , was assumed to be zero. Provided there is a large difference between the length scales of the coherent and incoherent motions (STRANGE and CRIGHTON [19]), the incompressible Navier–Stokes equation can be used with the triple-decomposition to yield nonlinear equations for the wave motion (ÖZDEMİR [20]). Linearisation of such equations implies that the space-time evolution of one wavenumber associated with a given eddy size will not affect that of the others so that the coherent structures develop independently. Although the question often arises as to the extent of validity of linearised theory, MICHALKE [12] points out that the error due to the linearisation of the disturbance equations is larger for higher disturbance frequencies than for lower ones. This justifies the present linear analysis since the frequencies measured in the wall jet were fairly low.

Provided that the deterministic motion is associated with the discrete part of the spectrum accessible by the modal equations, the coherent components of fluid motion can be represented by instability modes even though the set is not complete (BETCHOV and CRIMINALE [21], DRAZIN and REID [22]). For the present analysis, disturbances travelling and evolving in the basic flow direction were of interest and, since the growth rates obtained from a stability calculation for temporally growing disturbances cannot be transformed linearly with the phase velocity into spatial growth rates (MICHALKE [12]), solutions to the linearised equations can be assumed of the form

$$(2.2) \quad \begin{aligned} \tilde{u}_r &= A_r(z) \exp\{i(\alpha r - \beta t + m\phi)\} + (*), \\ \tilde{u}_\phi &= A_\phi(z) \exp\{i(\alpha r - \beta t + m\phi)\} + (*), \\ \tilde{u}_z &= A_z(z) \exp\{i(\alpha r - \beta t + m\phi)\} + (*), \\ \tilde{p} &= A_p(z) \exp\{i(\alpha r - \beta t + m\phi)\} + (*), \end{aligned}$$

where (*) refers the complex-conjugate term, A_r , A_z , A_ϕ , and A_p are the (complex) amplitude modulation functions of \tilde{u}_r , \tilde{u}_z , \tilde{u}_ϕ , and \tilde{p} , respectively. β is the real-valued circular-frequency ($2\pi f$) and α is the complex wavenumber defined as

$$\alpha = \alpha_r + i\alpha_i,$$

where α_r is the spatial wavenumber ($2\pi/\lambda$), and α_i is the rate of spatial evolution of a given component. It should also be pointed out that the curvilinear coordinate, ϕ , introduces a direction which can permit the evolution of the discrete

azimuthal modes of instability similar to the helical modes of the axisymmetric shear layer (STRANGE and CRIGHTON [19], PLASCHKO [23], COHEN and WYGNANSKI [24]). Indeed, the azimuthal instability modes of the wall jet flow could be a continuation of the helical shear layer structures of the inflowing jet which were, in some cases, known to survive after impingement (WIDNALL and TSAI [25], LUGT [26]) leading to large correlation between the wall jet and inflowing jet turbulence. The above formulation, therefore, accounts for the presence of the spinning modes (with azimuthal wavenumber, m) which, in some cases, have been as unstable as the axisymmetric modes (COHEN and WYGNANSKI [24]).

Since the stability of the flow is a local characteristic, the radial velocity maximum, $\bar{U}_{r,M}(r, \phi)$, has to be selected as the velocity scale, and the wall distance, z , is assumed to scale with the half-velocity thickness, $z_{0.5}$. It was shown by ÖZDEMİR [27] that the azimuthal symmetry of the wall flow was distorted due to the angled impingement of the inflowing jet and, therefore, it was necessary to take into account the azimuthal variation of the radial spreading. However, transforming the distorted coordinates of the wall jet flow of the angled impingement to those of the normal impingement, which can be treated analytically by the cylindrical coordinate system centered at the geometrical impingement point, required knowledge of the function relating the azimuthal and radial coordinates, which is difficult to deduce from the contour plots of surface pressure, as for example ÖZDEMİR and WHITELAW [5] (their Fig. 2.6). Here a heuristic approach was followed in which the radial distance from the geometrical impingement point, r , is assumed to scale with a so-called wetted radius, $r_w(\theta, \phi)$, which varies azimuthally as

$$(2.3) \quad r_w(\theta, \phi) = H \left\{ \sin(\theta \cos \phi) + \cos(\theta \cos \phi) \tan(\theta \cos(180 - \phi) + \gamma) \right\},$$

where γ is half the cone angle of the spread of the inflowing jet and was taken as 15 degrees from the flow visualisation pictures. The distributions of r_w are shown for $\theta = 0$ and 20 degrees in Fig. 2 and assumes elliptical shapes with

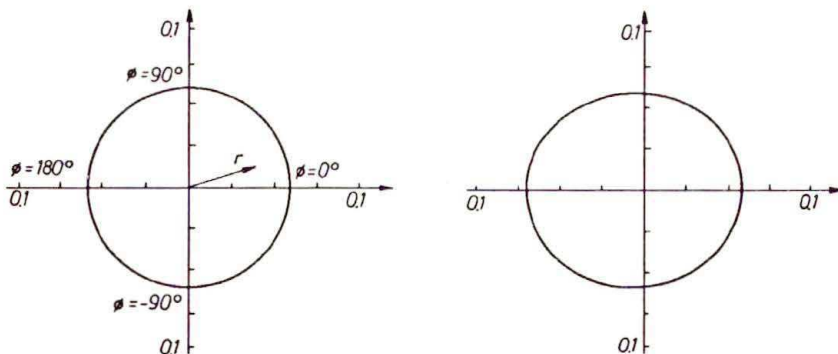


FIG. 2. Polar plot of the azimuthal distributions of the wetted radius for the impingement angles of $\theta = 0$ and 20 degrees.

increasing distance to the geometrical impingement point along the $\phi = 180$ -degree direction as impingement deviates from normal.

Further simplification of the formulation occurs when Reynolds number is large so that the viscous effects become very small, finally leading to

continuity:

$$(2.4)_1 \quad i\alpha^* A_r^* + \frac{z_{0.5}}{r^* r_w} A_r^* + \frac{im^* z_{0.5}}{r^* r_w} A_\phi^* + \frac{dA_z^*}{dz} = 0,$$

r -momentum:

$$(2.4)_2 \quad -i\beta^* A_r^* + i\alpha^* \bar{U}_r^* A_r^* + \frac{z_{0.5}}{r_w} \left(\frac{\bar{U}_r^*}{\bar{U}_{r,M}} \frac{\partial \bar{U}_{r,M}}{\partial r^*} + \frac{\partial \bar{U}_r^*}{\partial r^*} \right) A_r^* \\ + \frac{z_{0.5}}{r^* r_w} \left(\frac{\bar{U}_r^*}{\bar{U}_{r,M}} \frac{\partial \bar{U}_{r,M}}{\partial \phi} + \frac{\partial \bar{U}_r^*}{\partial \phi} \right) A_\phi^* + \bar{U}_z^* \frac{dA_r^*}{dz^*} + \frac{\partial \bar{U}_r^*}{\partial z^*} A_z^* + i\alpha^* A_p^* = 0,$$

ϕ -momentum:

$$(2.4)_3 \quad -i\beta^* A_\phi^* + i\alpha^* \bar{U}_r^* A_\phi^* + \frac{\bar{U}_r^* z_{0.5}}{r^* r_w} A_\phi^* + \bar{U}_z^* \frac{dA_\phi^*}{dz^*} + \frac{im^* z_{0.5}}{r^* r_w} A_p^* = 0,$$

z -momentum:

$$(2.4)_4 \quad -i\beta^* A_z^* + i\alpha^* \bar{U}_r^* A_z^* + \frac{z_{0.5}}{r_w} \left(\frac{\bar{U}_z^*}{\bar{U}_{r,M}} \frac{\partial \bar{U}_{r,M}}{\partial r^*} + \frac{\partial \bar{U}_z^*}{\partial r^*} \right) A_r^* \\ + \frac{z_{0.5}}{r^* r_w} \left(\frac{\bar{U}_z^*}{\bar{U}_{r,M}} \frac{\partial \bar{U}_{r,M}}{\partial \phi} + \frac{\partial \bar{U}_z^*}{\partial \phi} \right) A_\phi^* + \bar{U}_z^* \frac{dA_z^*}{dz^*} + \frac{\partial \bar{U}_z^*}{\partial z^*} A_z^* + \frac{dA_p^*}{dz^*} = 0.$$

Letting $A_r^* = Y_1$, $A_\phi^* = Y_2$, $A_z^* = Y_3$, $A_p^* = Y_4$, and rearranging, the following set of first-order ordinary differential equations can be obtained

$$(2.5) \quad \frac{dY_1}{dz^*} = \frac{1}{\bar{U}_z^*} \left\{ i\beta^* Y_1 - i\alpha^* \bar{U}_r^* Y_1 - \frac{z_{0.5}}{r_w} \left(\frac{\bar{U}_r^*}{\bar{U}_{r,M}} \frac{\partial \bar{U}_{r,M}}{\partial r^*} + \frac{\partial \bar{U}_r^*}{\partial r^*} \right) Y_1 \right. \\ \left. - \frac{z_{0.5}}{r^* r_w} \left(\frac{\bar{U}_r^*}{\bar{U}_{r,M}} \frac{\partial \bar{U}_{r,M}}{\partial \phi} + \frac{\partial \bar{U}_r^*}{\partial \phi} \right) Y_2 - \frac{\partial \bar{U}_r^*}{\partial z^*} Y_3 - i\alpha^* Y_4 \right\}, \\ \frac{dY_2}{dz^*} = \frac{1}{\bar{U}_z^*} \left\{ i\beta^* Y_2 - i\alpha^* \bar{U}_r^* Y_2 - \frac{\bar{U}_r^* z_{0.5}}{r^* r_w} Y_2 - \frac{im^* z_{0.5}}{r^* r_w} Y_4 \right\}, \\ \frac{dY_3}{dz^*} = -i\alpha^* Y_1 - \frac{z_{0.5}}{r^* r_w} Y_1 - \frac{im^* z_{0.5}}{r^* r_w} Y_2,$$

$$\begin{aligned}
 (2.5) \quad \frac{dY_4}{dz^*} = & i\beta^*Y_3 - i\alpha^*\bar{U}_r^*Y_3 - \frac{z_{0.5}}{r_w} \left(\frac{\bar{U}_z^*}{\bar{U}_{r,M}} \frac{\partial \bar{U}_{r,M}}{\partial r^*} + \frac{\partial \bar{U}_z^*}{\partial r^*} \right) Y_1 \\
 [\text{cont.}] \quad & - \frac{z_{0.5}}{r^*r_w} \left(\frac{\bar{U}_z^*}{\bar{U}_{r,M}} \frac{\partial \bar{U}_{r,M}}{\partial \phi} + \frac{\partial \bar{U}_z^*}{\partial \phi} \right) Y_2 \\
 & + \bar{U}_z^* \left(i\alpha^*Y_1 + \frac{z_{0.5}}{r^*r_w}Y_1 + \frac{im^*z_{0.5}}{r^*r_w}Y_2 \right) - \frac{\partial \bar{U}_z^*}{\partial z^*}Y_3.
 \end{aligned}$$

Note that when $\bar{U}_z^* \rightarrow 0$, Eqs. (2.5)_{1,2} have singularities which were introduced by disregarding the terms in Re^{-1} . The singularity due to diminishing value of \bar{U}_z^* occurs at the wall ($z^* = 0$) and can occur at an interior point if there is a local vertical flow reversal within the flow domain. Indeed, the vertical flow reversal in radial wall jet was first observed by LANDRETH and ADRIAN [3], and there is a clear evidence that flow reversal becomes stronger in oblique impingement (ÖZDEMİR and WHITELAW [5]). The difficulties associated with the singularity are discussed in detail by ÖZDEMİR [27] and here the emphasis is given to one-dimensional mean flow for which the equations have no singularity. If the basic flow field is assumed to be locally parallel so that \bar{U}_r^* is the only velocity component of the undisturbed wall jet, with $\bar{U}_z^* = 0$ everywhere, the set (2.5) further simplifies to

$$\begin{aligned}
 (2.6) \quad \frac{dY_3}{dz^*} = & -i\alpha^*Y_1 - \frac{z_{0.5}}{r^*r_w}Y_1 - \frac{im^*z_{0.5}}{r^*r_w}Y_2, \\
 \frac{dY_4}{dz^*} = & i\beta^*Y_3 - i\alpha^*\bar{U}_r^*Y_3
 \end{aligned}$$

with Y_1 and Y_2 defined as

$$\begin{aligned}
 (2.6') \quad Y_1 = & \left\{ \frac{z_{0.5}}{r^*r_w} \left(\frac{\bar{U}_r^*}{\bar{U}_{r,M}} \frac{\partial \bar{U}_{r,M}}{\partial \phi} + \frac{\partial \bar{U}_r^*}{\partial \phi} \right) Y_2 + \frac{\partial \bar{U}_r^*}{\partial z^*}Y_3 + i\alpha^*Y_4 \right\} \\
 & \cdot \frac{1}{i\beta^* - i\alpha^*\bar{U}_r^* - \frac{z_{0.5}}{r_w} \left(\frac{\bar{U}_r^*}{\bar{U}_{r,M}} \frac{\partial \bar{U}_{r,M}}{\partial r^*} + \frac{\partial \bar{U}_r^*}{\partial r^*} \right)}, \\
 Y_2 = & \left(\frac{im^*z_{0.5}}{r^*r_w}Y_4 \right) / \left(i\beta^* - i\alpha^*\bar{U}_r^* - \frac{\bar{U}_r^*z_{0.5}}{r^*r_w} \right).
 \end{aligned}$$

3. Mean flow, boundary conditions and solution procedure

In order to obtain the full transverse eigensolution at each radial position, the coefficients of the modal equations, which are functions of the mean flow parameters, are required. The streamwise development of the mean flow, therefore, affects the evolution of the instability modes, which has been considered with

multi-scale expansions defining the divergence of the mean flow (GASTER [15], CRIGHTON and GASTER [16], PLASCHKO [23]) and, since the local mean velocity profiles are the results of the nonlinear interactions, an implicit nonlinearity is imposed on the solutions. In the present analysis, mean flow parameters and their variations were provided in the form of empirical relations (ÖZDEMİR and WHITELAW [5]) as representatives of the pseudolaminar motion upon which the perturbations were superimposed. The mean radial velocity profiles nondimensionalised by the local maximum were similar at large radial distances

$$(3.1) \quad \bar{U}_r^* = \frac{\bar{U}_r}{\bar{U}_{r,M}} = \frac{(z/z_{0.5})^{\eta-1}}{\left(\frac{\eta-1}{\eta}\right)^{(\eta-1)/\eta} (\sqrt{2}s)^{\eta-1}} \exp \left\{ - \left(\frac{z/z_{0.5}}{\sqrt{2}s} \right)^\eta + \frac{\eta-1}{\eta} \right\}$$

(see also Table 1) with the streamwise evolution represented by

Table 1. Variation of η and s .

ϕ ($^\circ$):	0	90	180
η :	1.42	1.38	1.32
s :	0.54	0.52	0.54

$$(3.2) \quad \bar{U}_{r,M} = \tau(r-\zeta)^p \exp \left\{ - \left(\frac{r-\zeta}{\sqrt{2}\sigma} \right)^\tau \right\} / (\sqrt{2}\sigma)^\tau$$

which fits the experimental data (Fig. 3 and Table 2).

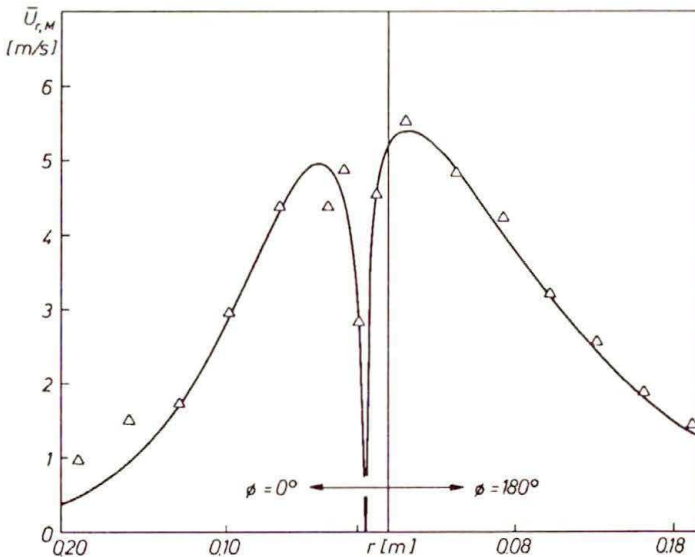


FIG. 3. Variation of the maximum of the mean radial velocity along the line of incidence.

Table 2. Parameters of Eq. (3.2).

ϕ (°):	0	180
ζ :	0.015	-0.015
p :	0.49	0.22
τ :	1.26	1.15
σ :	0.045	0.078

The set of first-order differential equations requires a condition to be specified for each equation to obtain the transverse eigensolution. The vertical velocity component at the wall should be zero due to the impermeable plate and, thus,

$$(3.3) \quad A_z^* = 0 \quad \text{at} \quad z^* = 0.$$

The eigensolution is defined over a semi-infinite interval [$z^* = 0, z^* = \infty$] with the upper boundary occurring at infinity but, for numerical purposes, it was replaced by a finite interval in which the condition at $z^* = \infty$ was assumed to occur at some finite $z^* = z_\infty^*$, so that the domain of the transverse eigensolution was forced to coincide with that of the mean flow where $\bar{U}_r^* = 0$ and the pressure attained the ambient value, i.e.,

$$(3.3') \quad A_p^* = 0 \quad \text{at} \quad z^* = z_\infty^*.$$

The eigenvalue problem defined in Eqs. (2.6) includes two coupled first-order linear ordinary differential equations. The solution was sought for the eigenvalues, α , and the corresponding transverse eigensolutions, $Y_k(z^*, \alpha)$, given the mean-flow parameters and the values of β and m . The solution procedure was similar to that of KELLER [28] with the reformulation of the equations, resulting in a nonlinear two-point boundary value problem. In order to avoid the growing solutions during the integration through the entire domain (BETCHOV and CRIMINALE [21]), the length of the domain of integration was divided into two in which a parallel shooting algorithm was used with the integration proceeding to an intermediate point by launching initial guesses from both ends of the interval and a matching of the solutions at the midpoint. The computations were performed on a DEC 5000 workstation in double precision and iterations for the multidimensional Newton-Raphson root finding technique concluded when the discrepancy vector was within some specified accuracy (typically 10^{-15}).

4. Numerical results and comparisons with experiments

For the first ten azimuthal modes and temporal frequency from 0 to 100 Hz, the set of inviscid equations (2.6) was solved along the line of impingement at radial positions where the experimentally observed vortices were most apparent

and the mean radial velocity achieved the similar form. The nondimensional amplification rates at $r/r_w = 2.274$ along the $\phi = 0$ degree direction, Fig. 4 a, are negative for all the waves considered, indicating decaying characteristics. Except for the axisymmetric ($m = 0$) and the first three helical modes ($m = \pm 1, \pm 2$ and ± 3), the curves show similar trends where $-\alpha_i z_{0.5}$ first increases with f and tends to a constant value which is lower for higher helical modes. For these four exceptions, there is a slight peak at around 7.5 Hz before the subsequent fall to a constant level, indicating a narrow range of frequencies at the lower end of the spectrum with the least damping relative to the other waves. It is interesting to note that the axisymmetric and the first helical modes have almost the same frequency response, which is consistent with the findings of COHEN and WYGNANSKI [24]. In order to trace the evolution of the waves, with attenuation occurring in the streamwise direction, the calculations were repeated for $r/r_w = 3.324$ and the results of Fig. 4 b show similar trends but, as would be expected, the least damped wave was shifted to a lower frequency, $f = 3.1$ Hz. This is consistent with the measured spatial evolution of the one-dimensional spectrum of radial fluctuation component of ÖZDEMİR and WHITELAW [5] in which a discrete frequency of 3.25 Hz was dominant at the same radial position. The results show that an increase of the width of the shear layer with the corresponding decrease in the mean energy along the streamwise direction, is accompanied by a negative amplification rate, i.e., attenuation with a continuous shift of the least attenuated instability waves towards lower frequencies.

The wavenumber-frequency spectra of Fig. 5 reveal that the wavenumbers are positive in the frequency range, where $-\alpha_i z_{0.5}$ has a maximum, and that a phase reversal occurs for the axisymmetric and some helical modes ($-6 \leq m \leq 6$), so that negative wavenumbers at large frequencies indicate upstream moving waves. The least attenuated waves move downstream with a positive phase velocity and indicate convection of the coherent turbulence along the mainstream with a decay quantified by the rate of attenuation of the waves. The relatively higher attenuation of the upstream moving waves is interesting in that the propagation of disturbances from the edges of the wall jet cannot interfere with the turbulence structure of the wall flow, and this is consistent with the fact that wall jet is not dependent on the conditions downstream, but affected by the initial conditions of the inflowing jet even at large radial distances. It is clear that if different frequencies were dominant at different wall distances, a transversal (vertical) eigensolution structure with a phase reversal occurring at a certain wall distance could lead to a situation which would be similar to the spatial phase reversal observed by SATO [29].

An attempt was made to compare the calculated distribution of the one-sided power spectrum of the radial fluctuation intensity for axisymmetric structures ($m = 0$) with that of measurements at $r/r_w = 2.274$ and 3.324 along the $\phi = 0$ degree direction. From the Eq. (2.2)₁, with $\alpha = \alpha_r + i\alpha_i$, space-time variation of the radial fluctuation that would be measured with a probe fixed at a point in the

[651]

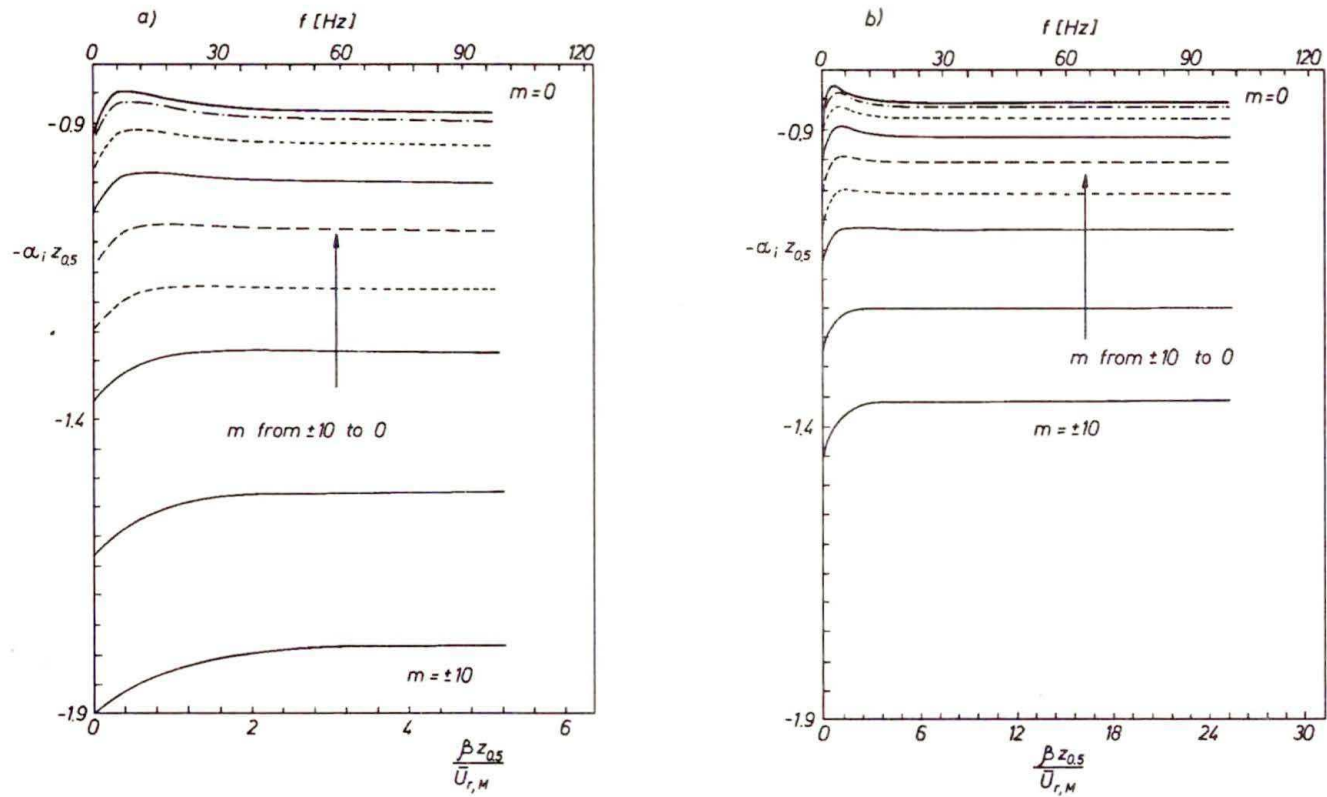


FIG. 4. Nondimensional amplification rates, a) $r/r_w = 2.274$ and b) $r/r_w = 3.324$.

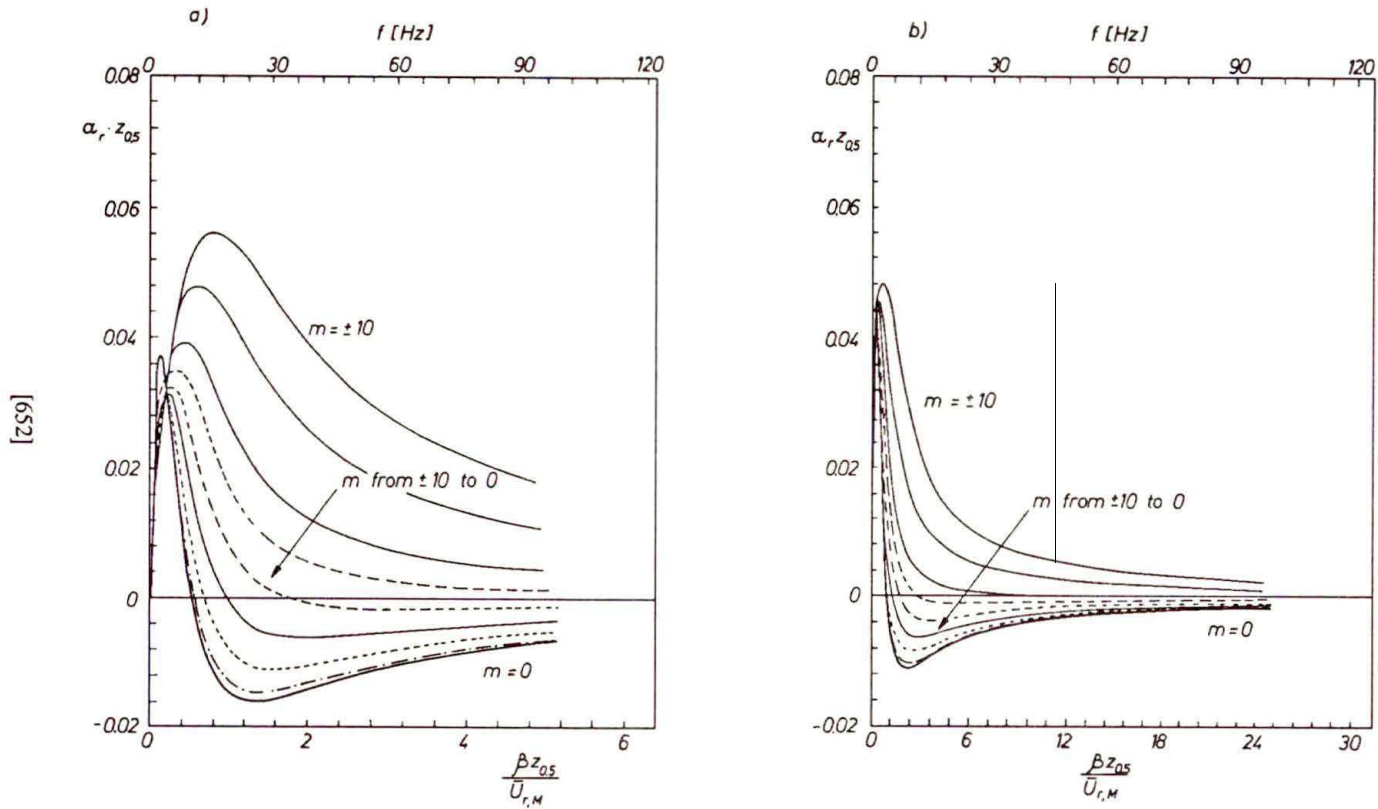


FIG. 5. Wavenumber-frequency spectrum, a) $r/r_w = 2.274$ and b) $r/r_w = 3.324$.

Eulerian coordinate, can be written as

$$(4.1) \quad \tilde{u}_r = [A_r(z) \exp \{i\alpha_r r - \alpha_i r + im\phi\}] \exp(-i\beta t) + (*),$$

where the term inside the bracket represents the complex amplitude of the vector rotating at a circular frequency β so that

$$(4.2) \quad \mathcal{F}(f) = A_r(z) \exp\{i\alpha_r r - \alpha_i r + im\phi\}.$$

As previously argued in Sec. 2, the complex conjugate term, (*), in Eq. (4.1) implies that each component at a frequency f is matched by a component at $-f$ which has equal amplitude so that, except for the case of $f = 0$, the total power associated with frequency, f , is given (RANDALL [30])

$$(4.3) \quad \mathbb{P}(f) = \frac{\mathcal{F}(f)^2}{2} = \frac{[A_r(z) \exp \{i\alpha_r r - \alpha_i r + im\phi\}]^2}{2}.$$

Since the eigenfunctions were determined except for the arbitrary multiplicative constant, the axis for the power spectrum in Figs. 6 and 7 has an arbitrary scale. A remarkable feature is that the large peak at the outer layer diminishes as the wall is approached and shifts towards slightly higher frequencies, and this is more evident in the contour plots. This trend is consistent with the measurements of ÖZDEMİR [27], where it was attributed to the restriction imposed on the growth of the inner vortex close to the wall by the outer free shear layer vortices, and the calculated values of the peak frequency are very close to those of the measurements particularly for $r/r_w = 3.324$.

Figure 8 shows radial fluctuation intensities calculated from the one-sided power spectrum with f ranging from 0 to 100 Hz for axisymmetric and spinning modes, $m = \pm 1, \pm 2, \pm 3, \pm 4, \pm 5, \pm 6, \pm 8$, and ± 10 at a radial position $r/r_w = 3.324$, where the radial fluctuation intensity completed its evolution towards two-peaked profile. By matching the amplitude of the radial velocity fluctuation component to the corresponding experimental value at the wall distance $z^* = 1.25$, favorable agreement was found between theory and experiment for the whole vertical eigenstructure of the radial fluctuation intensity, with large magnitudes occurring near the outer inflection point. The satisfactory agreement of the theoretical radial fluctuation intensity with the experiments was expected, since the slightly attenuated waves were known to correlate over a large distance of the order of the inverse of their damping ratio (LANDAHL [31]), and tend to dominate the non-wave-like disturbances and the whole turbulent flow field. The upper subfigure shows the relative contributions of different spinning modes with respect to the axisymmetric mode, so that the first helical mode is almost as important as the axisymmetric mode and the contribution was almost negligible for $m \geq 10$. It is also of interest to note that the calculations performed at the previous radial position, $r/r_w = 2.274$, along the $\phi = 0$ degree direction yielded

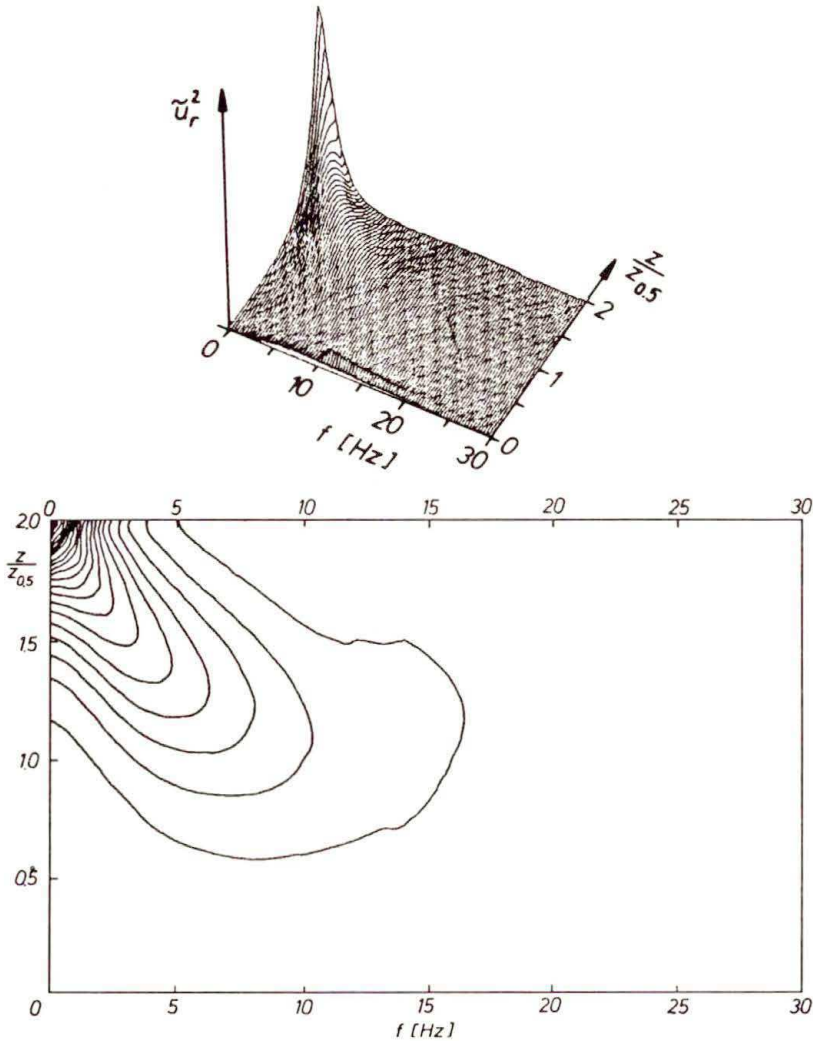


FIG. 6. One-sided power spectrum of radial fluctuation intensity for axisymmetric structures $m = 0$, $r/r_w = 2.274$ (\tilde{u}_r^2 axis has arbitrary scale).

very much the same fluctuation profile, although the measured fluctuation profile was different. Since the vertical mean profiles were different at these two radial positions, the results indicate that the mean radial velocity was dominant in the perturbed mean flow field but was not sufficient to describe the whole mean vorticity field which was responsible for the generation of the fluctuations (STUART [32]). Thus, it appears that the evolution of the mean vertical velocity needs to be included in the analysis to account for local changes of the fluctuation distribution when the streamwise component of the mean flow field was similar. Also, contrary to the stability calculations of BREWSTER and GEBHART [33] for natural

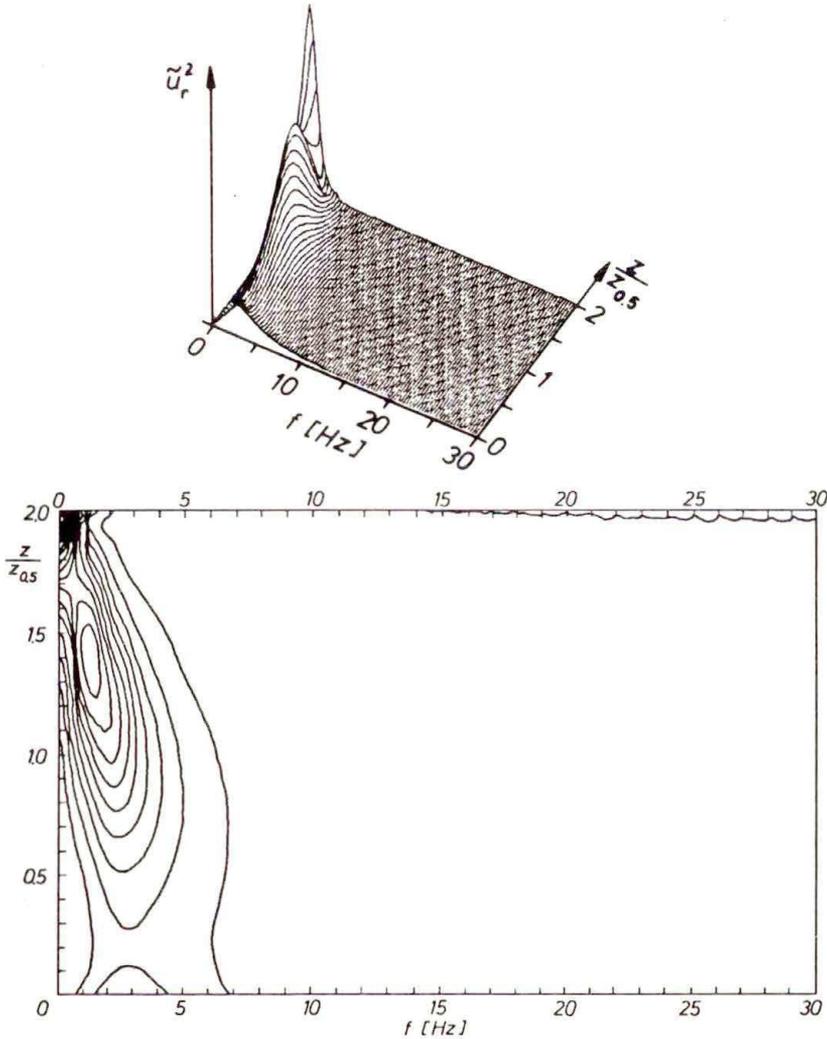


FIG. 7. One-sided power spectrum of radial fluctuation intensity for axisymmetric structures, $m = 0$, $r/r_w = 3.324$ (\tilde{u}_r^2 axis has arbitrary scale).

convection over a vertical hot plate, the present profiles of radial fluctuation intensity do not tend to diminish very close to the wall. This is to be expected since the present results are based on simplifications of inviscid equations.

Profiles of the induced pressure fluctuations, Fig. 9, reveal that the pressure fluctuations can attain a value of 63% at the wall. Again, the relative contributions of different azimuthal modes are similar to those of the radial fluctuation intensities. It is interesting to note that the radial velocity fluctuations exhibit far more structure than is displayed by the pressure fluctuations but, since pressure was not measured across the wall jet, it is difficult to be conclusive about the

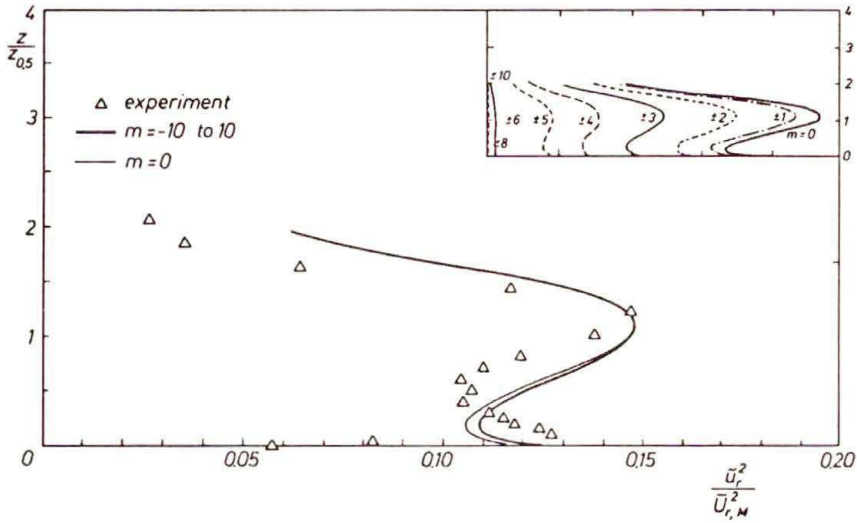


FIG. 8. Radial velocity fluctuation intensity for f from 0 to 100 Hz and m from 0 to ± 10 .

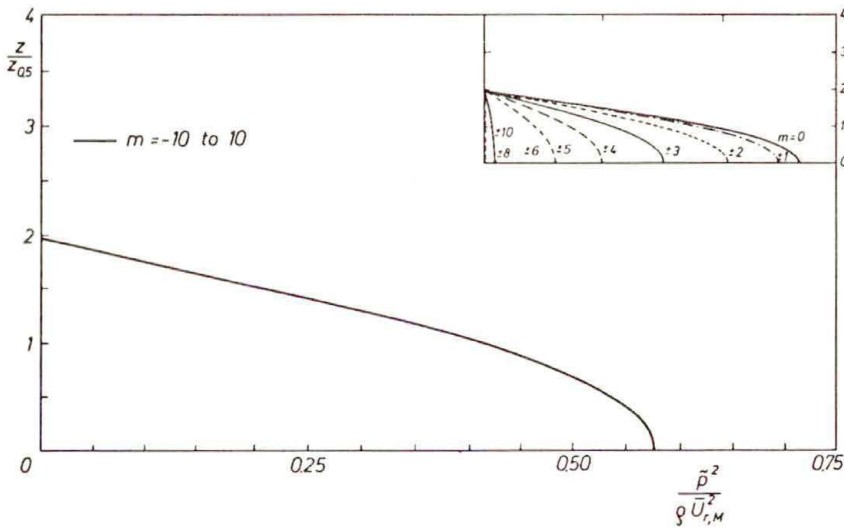


FIG. 9. Pressure fluctuation intensity for f from 0 to 100 Hz and m from 0 to ± 10 .

shape of the profiles. The azimuthal fluctuation intensity, on the other hand, exhibited a finite value at the wall and this violation of the no-slip condition must be due to that the fluctuation intensity was predicted by linear, inviscid stability analysis of one-dimensional basic flow, whereas the measured intensity was generated by apparently two-dimensional viscous basic flow. For the same reasons the agreement between vertical velocity fluctuations and the measured ones was poor.

5. Conclusions

The coherent turbulence characteristics of the radial wall jet were studied using discrete instability waves and linear analysis based on the assumption of a one-dimensional inviscid flow which was represented by time-averaged radial velocity. Calculations were performed in a region where the energy of mean flow was decaying so that the instability waves were attenuated with a phase reversal in frequency, in which the least attenuated waves were convected downstream while the others moved upstream. The trend of spectrum of the radial fluctuation component was well predicted with the dominant frequency shifted towards higher values close to the wall, and a good agreement was found in the evolution of the spectrum of radial fluctuation intensity in that the spectral information was closely correlated with the decay of the mean flow energy.

The shape of the calculated radial fluctuation intensity exhibited a trend with larger magnitudes at the outer inflection point, consistent with the experimentally observed array of vortices. The success of the inviscid predictions was attributed to the fact that the large coherent structures of the wall jet were associated with small wavenumbers, far remote from the viscous subrange, so that viscous dissipation did not play any important role in their dynamics (TOWNSEND [34]). However, the shape of the radial fluctuation intensity repeated itself at different positions despite the variation observed experimentally, and this led to the conclusion that the observed variations in the shape of intensity profiles were caused by the influences of the other components of the mean flow field and particularly the mean vertical velocity, whose profiles varied with the radial coordinate, even though the radial velocity profiles were similar. In other words, the mean vorticity was the determining factor for the overall performance of the stability predictions.

Acknowledgement

I am grateful to Professor J.H. WHITELAW of Imperial College for stimulating discussions which helped me to prepare this paper. The author has also greatly profited from the discussions with Professor J.T. STUART of Department of Mathematics of IC and, accordingly, thanks for bringing several references to the author's attention.

References

1. C. M. HO and N.S. NOSSEIR, *Large coherent structures in an impinging jet*, [in:] *Turbulent Shear Flows 2*, J.S.L. BRADBURY, F. DURST, B.E. LAUNDER, F.W. SCHMIDT and J.H. WHITELAW [Eds.], Springer-Verlag, 297–304, 1980.
2. C.M. HO and N.S. NOSSEIR, *Dynamics of an impinging jet. Part 1. The feedback phenomenon*, *J. Fluid Mech.*, **105**, 119–142, 1981.
3. C.C. LANDRETH and R.J. ADRIAN, *Impingement of a low Reynolds number turbulent jet onto a flat plate at normal incidence*, *Exp. Fluids*, **9**, 74–84, 1990.

4. M. POREH, Y.G. TSUEI and J.E. CERMAK, *Investigation of a turbulent radial wall jet*, J. Appl. Mech., **34**, 457–463, 1967.
5. İ.B. ÖZDEMİR and J.H. WHITELAW, *Impingement of an axisymmetric jet on unheated and heated flat plates*, J. Fluid Mech., **240**, 503–532, 1992.
6. N. DIDDEN and C.M. HO, *Unsteady separation in an impinging jet*, J. Fluid Mech., **160**, 235–256, 1985.
7. C.M. HO and P. HUERRE, *Perturbed free shear layers*, Ann. Rev. Fluid Mech., **16**, 365–424, 1984.
8. N. GREGORY, J.T. STUART and W.S. WALKER, *On the stability of three-dimensional boundary layers with application to the flow due to a rotating disk*, Phil. Trans. R. Soc. Lond., A **248**, 155–199, 1955.
9. J.T. STUART, *Hydrodynamic stability*, [in:] Laminar Boundary Layers, L. ROSENHEAD [Ed.], Clarendon Press, 492–579, 1963.
10. L.N. HOWARD, *The number of unstable modes in hydrodynamic stability problems*, J. Mécanique, **3**, 433–443, 1964.
11. Y. TSUI, Y. MORIKAWA, T. NAGATANI and M. SAKOU, *The stability of a two-dimensional wall jet*, Aeronaut. Q., **28**, 235–246, 1977.
12. A. MICHALKE, *On spatially growing disturbances in an inviscid shear layer*, J. Fluid Mech., **23**, 521–544, 1965.
13. A. MICHALKE and G. HERMANN, *On the inviscid instability of a circular jet with external flow*, J. Fluid Mech., **114**, 343–359, 1982.
14. M. BOUTHIER, *Stabilité linéaire des écoulements presque parallèles*, J. Mécanique, **11**, 599–621, 1971.
15. M. GASTER, *On the effects of boundary-layer growth on flow stability*, J. Fluid Mech., **66**, 465–480, 1974.
16. D.G. CRIGHTON and M. GASTER, *Stability of slowly divergent flow*, J. Fluid Mech., **77**, 397–413, 1976.
17. A.K.M.F. HUSSAIN, *Coherent structures – reality and myth*, Phys. Fluids, **26**, 2816–2850, 1983.
18. A.K.M.F. HUSSAIN and W.C. REYNOLDS, *The mechanics of an organised wave in turbulent shear flow*, J. Fluid Mech., **41**, 241–258, 1970.
19. P.J.R. STRANGE and D.G. CRIGHTON, *Spinning modes on axisymmetric jets. Part 1*, J. Fluid Mech., **134**, 231–245, 1983.
20. İ.B. ÖZDEMİR, *Stability of the wall jet*, Section report MFMAD/95/4, Mechanics Division, School of Mech. Engng., İTU, 1995.
21. R. BETCHOV and W.O. CRIMINALE, *Stability of parallel flows*, Academic Press., 1967.
22. P.G. DRAZIN and W.H. REID, *Hydrodynamic stability*, Cambridge Univ. Press., 1981.
23. P. PLASCHKO, *Helical instabilities of slowly divergent jets*, J. Fluid Mech., **92**, 209–215, 1979.
24. J. COHEN and I. WYGNAŃSKI, *The evolution of instabilities in the axisymmetric jet. Part 1. The linear growth of disturbances near the nozzle*, J. Fluid Mech., **176**, 191–219, 1987.
25. S.E. WIDNALL and C.Y. TSAI, *The instability of the thin vortex ring of constant vorticity*, Phil. Trans. R. Soc. Lond., A **287**, 273–305, 1977.
26. H.J. LUGT, *Vortex flow in nature and technology*, Wiley, 1983.
27. İ.B. ÖZDEMİR, *Impingement of single and two-phase jets on unheated and heated flat plates*, Ph.D. Thesis, Imperial College, London 1992.
28. H.B. KELLER, *Numerical solution of two-point boundary value problems*, CBMS-NSF Regional Conference Series in Applied Mathematics, vol. 24, 1976.
29. H. SATO, *Further investigation on the transition of two-dimensional separated layer at subsonic speeds*, J. Phys. Soc. Japan, **14**, 1797–1810, 1959.
30. R.B. RANDALL, *Frequency analysis; Application to B&K equipment*, Brüel and Kjaer, 1977.
31. M. LANDAHL, *A wave-guide model for turbulent shear flow*, J. Fluid Mech., **29**, 441–459, 1967.
32. J.T. STUART, *Course notes on Hydrodynamic Stability*, Department of Mathematics, Imperial College, 1989.
33. R.A. BREWSTER and B. GEBHART, *Instability and disturbance amplification in a mixed-convection boundary layer*, J. Fluid Mech., **229**, 115–133, 1991.
34. A.A. TOWNSEND, *The structure of turbulent shear flow*, Cambridge Univ. Press., 1976.

İSTANBUL TECHNICAL UNIVERSITY
SCHOOL OF MECHANICAL ENGINEERING
MECHANICS DIVISION, İSTANBUL, TURKEY.

Received October 9, 1995.